JACS
JOURNAL OF THE AMERICAN CHEMICAL SOCIETY
Article
pubs.acs.org/JACS

Ligand–Receptor Interaction Modulates the Energy Landscape of Enzyme-Instructed Self-Assembly of Small Molecules

Richard Haburcak,[†] Junfeng Shi,[†] Xuewen Du, Dan Yuan, and Bing Xu*

Department of Chemistry, Brandeis University, 415 South Street, MS 015, Waltham, Massachusetts 02453, United States

Supporting Information

ABSTRACT: The concurrence of enzymatic reaction and ligand–receptor interactions is common for proteins, but rare for small molecules and has yet to be explored. Here we show that ligand–receptor interaction modulates the morphology of molecular assemblies formed by enzyme-instructed assembly of small molecules. While the absence of ligand–receptor interaction allows enzymatic dephosphorylation of a precursor to generate the hydrogelator that self-assembles to form long nanofibers, the presence of the ligand–receptor interaction biases the pathway to form precipitous aggregates containing short nanofibers. While the hydrogelators self-assemble to form nanofibers or nanoribbons that are unable to bind with the ligand (i.e., vancomycin), the addition of surfactant breaks up the assemblies to restore the ligand–receptor interaction. In addition, an excess amount of the ligands can disrupt the nanofibers and result in the precipitates. As the first example of the use of ligand–receptor interaction to modulate the kinetics of enzymatic self-assembly, this work not only provides a solution to evaluate the interaction between aggregates and target molecules but also offers new insight for understanding the emergent behavior of sophisticated molecular systems having multiple and parallel processes.

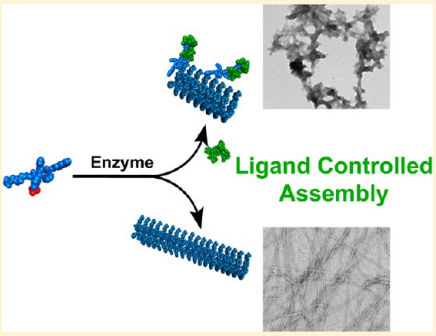

INTRODUCTION

This article reports the first use of the ligand–receptor interaction to regulate enzymatic self-assembly and emergent properties of the assemblies of small molecules. Self-assembly of small molecules is a thermodynamically favorable process during which small molecule monomers assemble to form large supramolecular structures.[1−9] Typically these supramolecular structures are static with properties dictated by their constituents.[4] In nature, however, it is dynamic supramolecular structures and emergent properties of the assemblies which are the most prevalent.[10,11] A prominent process is reversible protein phosphorylation and dephosphorylation that regulates many essential cellular functions.[12] For example, tyrosine phosphorylation in VAV protein is a key mechanism in regulating the ligand–receptor interaction, thus further activating enzymes for immune responses.[13] Additionally, the complex protein folding process has a well-established reliance on dephosphorylation of ATP by chaperone proteins.[14,15] Meanwhile, immunological studies show that enzymatic transformation generates death ligands (e.g., TNF, TRAIL), which bind to cell death receptors to initiate oligomerization processes that control cell fates. A fundamental feature of these processes in living systems is the concurrence of enzymatic reaction and ligand–receptor interactions (e.g., enzymes or pseudo enzymes as molecular scaffolds for self-assembly),[16] which results in sophisticated control of protein–protein interactions. This fact raises the possibility of employing small molecules to mimic this essential process for modulating protein–protein interactions, which would be a novel strategy for developing new therapeutics. Despite their significance, such an approach has received limited exploration because of the limited number of well-defined ligand–receptor systems of small molecules. Recently, we reported that enzymatic reaction is able to dimerize the ligand to mimic the activation of signal transduction.[17] It would be highly desirable to use ligand–receptor interactions to modulate the outcome of enzyme-instructed self-assembly (EISA)[18−23] of small molecules because morphological differences of the nanoscale assemblies may elicit different cellular responses.[24−28] However, the use of ligand–receptor interactions for precisely controlling the kinetic behavior of small molecules remains challenging.

To understand the complex behavior of sophisticated molecular systems undergoing multiple and/or parallel processes, we choose to explore small molecules that are substrates of enzymes and are participants of ligand–receptor interactions. Specifically, we synthesized a small heptapeptide, Nap-FFYGGaa (**1**), which self-assembles to form nanofibers or nanosheets in aqueous solution. Phosphorylated **1** (i.e., **1P**, phosphorylated at tyrosine residue) is a substrate of alkaline phosphatase (ALP) and a receptor of vancomycin (**2**). Our study reveals that the assemblies of **1** exhibit emergent properties of assembled molecules,[29,30] which drastically affect the ligand–receptor interaction between the assemblies and the ligand, in effect "switching off" the ligand–receptor interaction between **2** and **1**. On the other hand, the ligand–receptor interaction between **2** and **1P** is able to bias EISA of **1** to generate aggregates containing short nanofibers, an observation

Received: July 25, 2016
Published: October 31, 2016

DOI: 10.1021/jacs.6b07677
J. Am. Chem. Soc. 2016, 138, 15397−15404

that differs from EISA of **1** in the absence of **2**. Additionally, during EISA of **1** in the presence of **2**, short fibers emerge first, followed by aggregation and disruption of fibers, leading to formation of a precipitate. This transient fiber formation is coupled with a time-dependent change in the viscoelastic properties of the solution of **1**, **2**, and ALP, which is not observed when one of the components is missing, the hallmark of emergent behavior. As shown in Scheme 1, immediately after

Scheme 1. Illustration of Ligand–Receptor Interaction of Small Molecules Dictating the Pathways of EISA

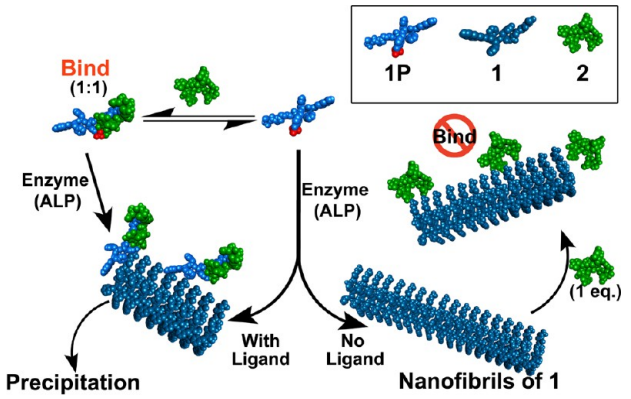

enzymatic dephosphorylation, **1** is "monomeric" and is able to bind the ligand (**2**), or the enzyme can dephosphorylate the complex of **1P** and **2**. Thus, the binding between **1** and **2** favors an alternative pathway of assembly (i.e., different from the supramolecular polymerization of **1** observed without **2**), leading to precipitation. While **2** shows no measurable binding to assemblies of **1**, the addition of a surfactant Tween-80 (Tw-80) breaks up the assemblies of **1** and restores binding between **1** and **2**. Isothermal titration calorimetry (ITC) measurement in the presence of surfactant, in fact, serves as a facile method to study interactions between ligands and receptors when either are prone to aggregate.

While proteins usually change their conformation or shape upon enzymatic reaction to regulate ligand–receptor interaction for specific functions, as shown in the case of inherently disordered proteins,[31,32] small molecules, in general, barely exhibit large conformational differences upon enzymatic reaction. As the first example illustrating reciprocal modulation between ligand–receptor interaction and enzymatic self-assembly, this work provides useful insights for developing nanoscale assemblies of small molecules for controlling biological and cellular processes, understanding the emergent behavior of sophisticated molecular systems undergoing multiple and parallel processes, and further offers a general approach to control the transformation of small molecules in the context of ligand–receptor interactions.

RESULTS AND DISCUSSION

Molecular Design and Synthesis. We chose vancomycin (**2**) and a D-Ala-D-Ala derivative (**1**) as the ligand–receptor pair because of their well-established and specific interactions, as demonstrated by Walsh,[33,34] Williams,[35] and Whitesides[36,37] as well as other groups.[38,39] Recently, we have shown that ligand–receptor interaction modulates the cytotoxicity of molecular aggregates.[40,41] Encouraged by these results, we designed a small molecule (Nap-FF$_p$YGGaa (**1P**)) and the hydrogelator **1**. The heptapeptide and various derivatives (Scheme 2) were synthesized by standard solid-phase peptide synthesis (SPPS)

Scheme 2. Molecular Structures of the Heptapeptidic Precursor 1P and Its Corresponding Hydrogelator 1

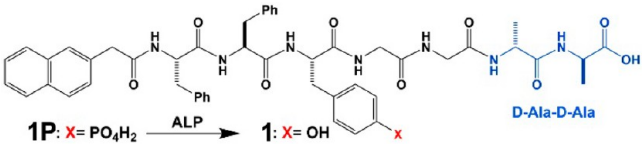

procedures (see Supporting Information (SI)) on a 2-chlorotrityl chloride resin,[42] further purified by HPLC on a reverse phase C18 column, and lyophilized to give the peptides as fine white powders in approximately 80% yield. Phosphorylated tyrosine was synthesized following previously reported methods[43] and the free amine further protected by an Fmoc group for SPPS. The overall yield of **1P** is about 80%, based on resin loading.

Ligand Modulates Enzymatic Self-Assembly. To understand how self-assembly affects the ligand–receptor interaction and how the ligand–receptor interaction modulates the process or behavior of enzymatic self-assembly, we used ALP to catalyze dephosphorylation of **1P** without and with the presence of **2**. As shown in Figure 1A, without ALP, the addition of 1 equiv of

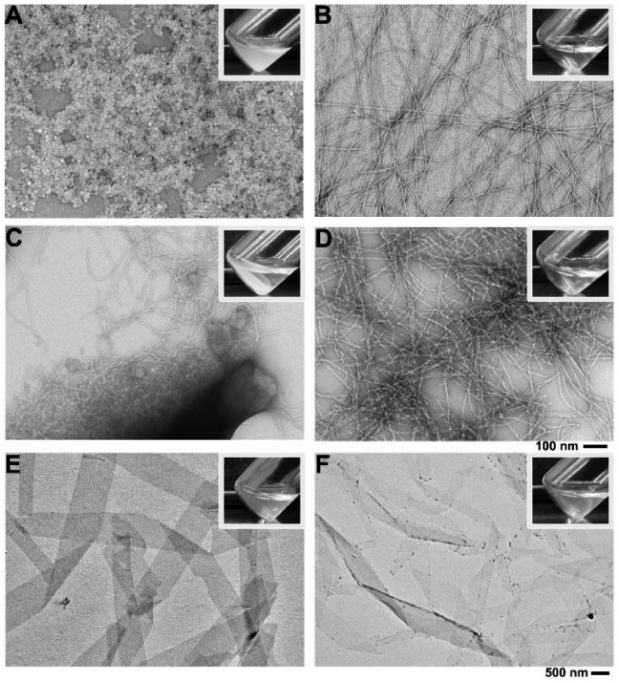

Figure 1. TEM images of (A) suspension of **1P** and **2**; (B) **1P** and ALP; (C) **1P**, **2**, and ALP; (D) **1P** treated with ALP for 2 days and then **2** was added; and (E) **1** and (F) **1** and **2** in water. $[\mathbf{1P}]_0 = [\mathbf{1}]_0 = [\mathbf{2}]_0 = 500\ \mu M$, ALP = 1.25 U/mL, pH = 7.4.

2 into the solution of **1P** (500 μM) results in a colloidal suspension, which forms precipitates depending on pH and concentration, indicating strong intermolecular interaction between **1P** and **2**. Transmission electron microscopy (TEM) shows that the morphology of the aggregates is largely unstructured (Figure 1A). In the absence of **2**, ALP (1.25 U/mL) converts **1P** to **1**, which, as expected, self-assembles to

DOI: 10.1021/jacs.6b07677
J. Am. Chem. Soc. 2016, 138, 15397–15404

form long nanofibers (Figure 1B). When the concentration of **1P** is 500 μM, the enzyme-induced formation of the nanofibers results in a viscous mixture. The simultaneous addition of **2** (1 equiv) and ALP (1.25 U/mL) into a solution of **1P** (500 μM) induces formation of large aggregates, which cluster together and form precipitates (Figure 1C) over time. Although a self-supporting gel was only made upon changing the pH of a 4 mM solution of **1** to pH 6.4 (Figure S2), the addition of ALP into the solution of **1P** (500 μM) and **2** (500 μM) also yields gel pieces that are sufficiently stable for rheology measurement (Figures S3 and S4). These results confirm that **1** is a hydrogelator. The formation of precipitates over time agrees with an observed decrease in the storage modulus or critical strain of the mixture over 24 h (Figure S3). Furthermore, the time dependence of the changes in storage and loss moduli are an emergent property of the combination of all three components. However, 2 days after using ALP to generate **1** from **1P**, the addition of 1 equiv of **2** to the solution of **1** hardly yields any precipitates after 24 h. TEM reveals that the nanofibers (Figure 1D) are similar to those formed by mixing **1P** and ALP without the post-self-assembly addition of **2**. This result indicates that, being a kinetically trapped state following EISA of **1**, the assemblies of **1** hardly favor binding with **2**. Interestingly, while the direct addition of **1** in water results in a suspension consisting of nanoribbons (Figure 1E), TEM reveals small unstructured aggregates on the edge of the nanoribbon of **1** after the addition of **2** (Figure 1F). On the other hand, the addition of 5 equiv of **2** into a 500 μM suspension of **1** almost completely destroys the nanoribbons formed by **1** and affords an opaque colloidal precipitate (Figure S5) 24−48 h after the addition, indicating that high concentrations of **2** shift the equilibrium toward binding between **1** and **2**.

ITC of Binding and Stability of the Assembly. To investigate the interaction between **2** and the D-Ala-D-Ala derivatives (i.e., **1P** and **1**), we used ITC to estimate the dissociation constant (K_d) of the binding between **1P** and **2**. As shown in Figure 2A, **1P** binds with **2** in a 1:1 ratio, with a K_d of 108 μM. This result agrees well with relatively tight binding between **2** and D-Ala-D-Ala. Titration in the presence of ALP appears to give a dissociation constant of 10 μM (Figure S6). This result suggests that the dephosphorylation process and subsequent self-assembly still permit the binding of **2** with **1P** or **1**. In contrast, assemblies of **1** hardly bind with **2**. The heating profile (Figure 2B) of titration of **2** into a suspension of **1** is similar to that of the dissociation of the dimers of **2** (Figure S7), suggesting that the interaction between assembled **1** and **2** is too weak to be measured by ITC. In fact, this is the first case where **2** shows negligible binding with a D-Ala-D-Ala derivative.

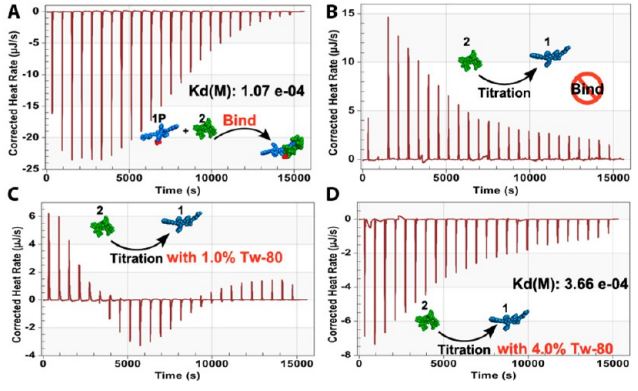

Figure 2. ITC of (A) **1P** and (B−D) **1** with **2** at different concentrations of Tw-80 for the determination of dissociation constant (K_d) and stoichiometry (n). Negative peaks indicate an exothermic release of heat.

Considering that the assemblies of a hydrogelator containing D-Ala-D-Ala,[17,44] in a previous report, are able to bind with **2**, the lack of binding between **2** and the assemblies of **1** is surprising. To understand this result, we synthesize control molecules Nap-ff$_p$yGGaa (**3P**) and the corresponding self-assembling molecule, **3**, by replacing the L-amino acid residues, FFY, in **1P** or **1**, with their D-amino acid enantiomers, ffy. Like **1P**, **3P** binds with **2** with a K_d of 82 μM. Similarly to the assemblies of **1**, the assemblies of **3** barely bind with **2** (Figure S8). This control experiment excludes the possibility that the conformation of the receptor (i.e., **1** or **3**) weakens the binding between **1** (or **3**) and **2**. Moreover, this result confirms that the assemblies of small molecules, indeed, differ considerably from their monomeric building blocks. As expected, upon the mutation of D-Ala-D-Ala to L-Ala-L-Ala, the resulting molecule, **4P** (or **4**), is unable to bind with **2** (Figure S8), which further confirms that the ligand−receptor interaction between **2** and **1P**, **1**, **3P**, or **3** still relies on the binding between vancomycin and D-Ala-D-Ala

To compare the complex parallel processes occurring during the ITC experiments and to gain insights into the supramolecular behavior observed in the TEM in Figure 1, we examined the total heat released over the entire ITC experiment. We carried out three sets of titrations (in PBS buffer and at pH 7.4): **1P** to (i) **2** alone, (ii) to ALP alone, and (iii) to a solution of **2** and ALP ($[ALP]_0$ = 1.67 U/mL). Integrating the heat release profiles for each titration yields the total heat released for each titration, from which the total heat released by dilution of **1P** is subtracted. The total heat release is −4261 μJ for titration of **1P** to **2**, −4653 μJ for titration of **1P** to ALP, and −7186 μJ for titration of **1P** to **2** and ALP (Figure S9), indicating that formation of nanofibers by dephosphorylation of **1P** is more enthalpically favorable than binding of **1P** and **2** alone. Importantly, the heat released from binding of **1P** and **2** is comparable to heat released from dephosphorylation of **1P**. This result agrees with hardly any disruption of fibers of **1** formed by dephosphorylation of **1P** following the addition of **2** (Figure 1D). However, the fibers of nanosheets of **1**, being kinetically trapped, can slowly transform over several weeks to months to a precipitate after the addition of 5 equiv of **2**. Furthermore, as the total heat released by titration of **1P** to a solution of **2** and ALP is significantly larger than the heat released by simple dephosphorylation of **1P**, **2** likely provides a low-energy intermediate along the fibrilization pathway of **1**, which drives the hydrogelator to form the unstructured aggregates that contain **1** and **2** (Figure 1C).

Addition of Surfactant Restores the Ligand−Receptor Interaction. A series of studies by Shoichet et al. have revealed that the aggregation of small molecules in water usually leads to false positives (up to 95%) in drug screening,[45,46] which certainly is a form of abnormal binding. In addition to indicating the aggregates of small molecules are a rather general phenomenon, those results also imply that the assemblies can cause false negatives (i.e., the lack of ligand−receptor binding between **2** and **1**). To verify that "monomeric" **1** still is able to bind to **2**, we employed a nonionic surfactant, Tw-80, to disrupt assemblies of **1**. In the presence of 1.0 wt % of Tw-80, the appearance of negative peaks in the ITC heating profile

DOI: 10.1021/jacs.6b07677
J. Am. Chem. Soc. 2016, 138, 15397−15404

indicates a release of heat (Figure 2C), likely due to molecular binding between **1** and **2**. Upon increasing the Tw-80 concentration to 4.0 wt %, heating release dominates the whole titration process (Figure 2D), and fitting by an independent binding model gives a dissociation constant of 366 μM. This result confirms that surfactant restores the ligand−receptor interaction between **2** and **1**. Moreover, this result suggests that using surfactant during ITC offers a facile method to study binding between ligands and aggregate-prone receptors. We further used ITC in the presence of Tw-80 to measure the binding of **2** and **3**. Similar to the case of **1**, the addition of 4.0 wt % Tw-80 recovers the ligand−receptor binding between **2** and **3** (Figure S10). In addition, the heating profile of the titration of **2** into a solution of **4** shows negligible change over various concentrations of Tw-80 (Figure S11). These results indicate that the surfactant itself has little contribution to heat released during the titrations shown in Figure 2C,D. The observed heat release likely originates from the interaction of **2** and the monomeric **1** after the surfactant disrupts the assemblies of **1**.

Surfactant Breaks the Assemblies and Restores Binding. To verify the effect of Tw-80 on assemblies of **1**, we used dynamic light scattering (DLS) to monitor the light scattering signal and hydrodynamic radius (R_h) of suspensions of **1** with different amounts of Tw-80 (Figure 3). As seen in

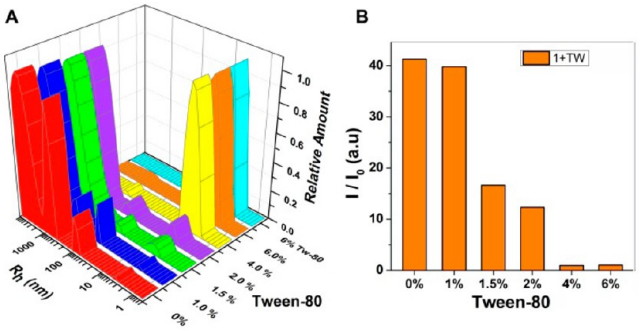

Figure 3. DLS measurements showing (A) hydrodynamic radii and (B) light scattering signals (I/I_0) for the solution of **1** (800 μM) with various concentrations of Tw-80 (wt %).

Figure 3A, as the Tw-80 concentration increases from 1.0 wt % to 2.0 wt %, a peak representing species with an R_h ranging from 3 to 10 nm starts to grow. When the concentration of Tw-80 is increased to 4.0 wt %, this peak exhibits significant growth, accompanied by the disappearance of the peaks corresponding to the assemblies (larger than 100 nm), indicating that the addition of Tw-80, indeed, disrupts the assemblies of **1**. Meanwhile, the light scattering signal of **1** decreases gradually with increasing Tw-80 concentration (Figure 3B). After the addition of 4.0 wt % Tw-80 into a suspension of **1**, the light scattering signal decreases significantly and is almost identical to a solution of 4.0 wt % Tw-80 alone (Figure S13). This result not only confirms that assemblies of **1** dissociate upon the addition of Tw-80 but also suggests that the dissociated species are too small to scatter light. TEM images (Figure 4) show that, at a higher Tw-80 concentrations, the long dense nanosheets of **1** become low density short nanosheets, with only a few small fibrils remaining. Finally, at 4.0 wt % Tw-80, nanoparticles dominate (Figure S15). These results confirm that Tw-80 disrupts the assemblies of **1** into oligomers.

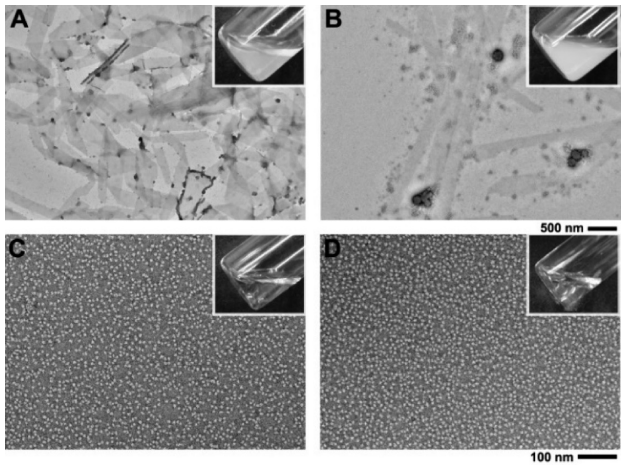

Figure 4. TEM images of suspensions of **1** and **2** with (A) 0 wt %, (B) 1.0 wt %, and (C) 4.0 wt % of Tw-80 or TEM of (D) only 4.0 wt % of Tw-80. Inset are their optical images. $[\mathbf{1}]_0 = [\mathbf{2}]_0 = 800$ μM.

After the DLS study of the effect of Tw-80 on assemblies, we used TEM to examine the morphological properties of **1** and **2** under various amounts of Tw-80. TEM micrographs of the colloidal solution of **1** and **2** show large amounts of nanosheets with dots along the edges, likely unstructured aggregates of **1** and **2**. The presence of nanosheets and relatively few aggregates agrees well with no measurable ligand−receptor interaction between **2** and assembled **1**. After adding 1.0 wt % Tw-80 into a suspension of **1** and **2**, more unstructured aggregates form, and nanosheets still remain (Figure 4B). Meanwhile, optical images clearly show the formation of precipitates. This result indicates that as 1.0 wt % Tw-80 breaks up assemblies of **1**, the oligomers released are able to bind with **2** to form aggregates, which bind together to form precipitates. Such an observation is consistent with our previous results that as **1P** is converted to **1**, the forming hydrogelator binds with **2** to induce aggregation. At 4.0 wt % Tw-80, the aggregates disappear to give a clear solution, consisting of nanoparticles with a diameter of 12 ± 2 nm (Figure 4C), which is almost identical to a solution only containing 4.0 wt % Tw-80. This result indicates that, due to the strong dissolution of Tw-80, the complex of **1** and **2** is unable to form large aggregates. Together with DLS data, this result also confirms that 4.0 wt % Tw-80 completely breaks up assemblies of **1** to monomeric or oligomeric **1**, which binds with **2** (i.e., restores the ligand−receptor interaction).

Morphological Evolution. As demonstrated for both small molecule supramolecular polymerization[41,47−49] and for assembly of amyloid proteins,[50−52] aggregate morphology, and even toxicity, has a strong dependence on initial conditions and the aggregation pathway. A time-dependent study of the gelation and precipitation behavior of **1P** in the presence of **2** and ALP reveals that the morphology and self-assembling behavior of **1** correlate with the concentration of **2**. As shown in Figure 5, the morphologies of the fibers or amorphous precipitates formed after the addition of **2** to a solution of **1P** and ALP exhibit a strong dependence on the concentration of **2**. The addition of 1 equiv of **2** is unable to prevent the formation of long nanofibers, but can turn the nanofibers into short fibers within 48 h, accompanied by forming a precipitate identical to that in Figure 1C. While the addition of 1.5 equiv of **2** decreases the nanofiber density, the addition of 2 or 3 equiv of **2** results in precipitation within 24 h. The addition of 5 equiv of **2** completely prevents the formation of long nanofibers.

DOI: 10.1021/jacs.6b07677
J. Am. Chem. Soc. 2016, 138, 15397−15404

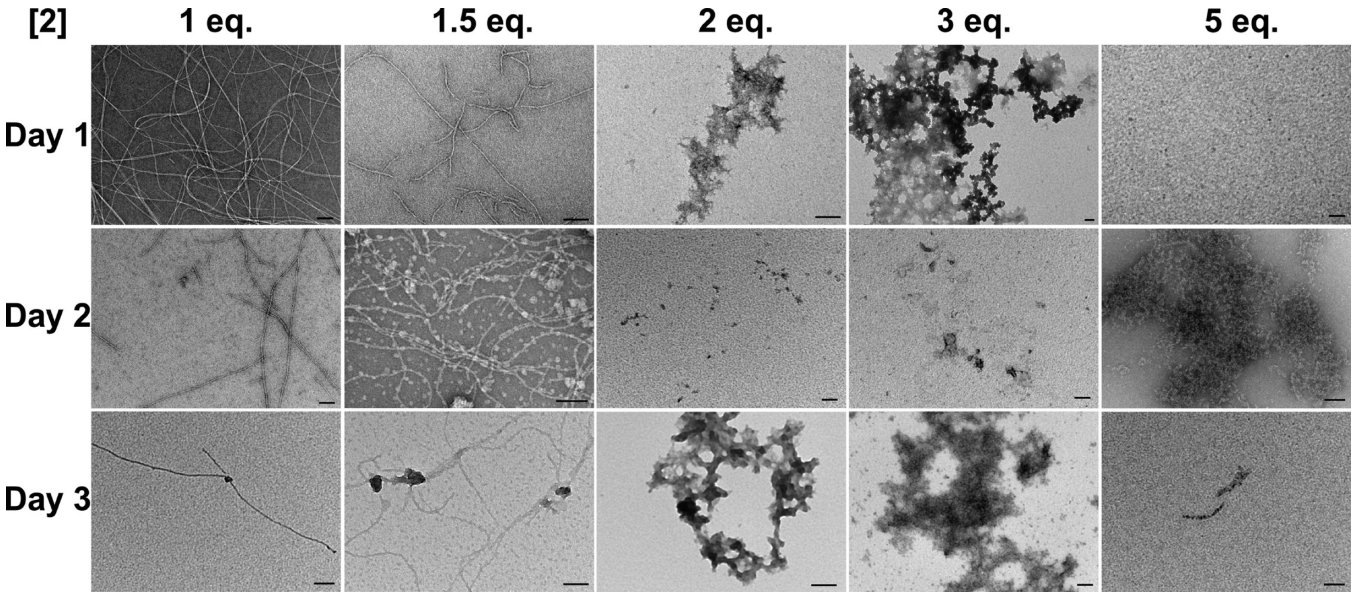

Figure 5. TEM micrographs taken on three consecutive days of suspensions of **1P**, **2**, and ALP, with varying concentrations of **2**. $[\mathbf{1P}]_o$ = 500 μM, ALP = 1.25 U/mL, pH = 7.6, each scale bar is 100 nm.

These results indicate that, at pH 7.6, nanofibers are a metastable state along the precipitation pathway, suggesting that the interaction between **1** and **2** leading to precipitation is indeed energetically more favorable than self-assembly of **1** alone.

Variation of ALP concentration gives similar results, with higher ALP concentrations giving rise to more dense nanofibers prior to precipitate formation (Figures 6 and S19). Surprisingly, at an ALP concentration of 6.25 U/mL, nanofibers remained on the third day, indicating increased order of the nanofibers of **1** formed at higher enzyme concentration, similar to enzyme-induced order of supramolecular polymerization reported by Ulijn et al.[18,53] There also is an alternative explanation to the stability of the fibers formed at 6.25 U/mL ALP. Higher enzyme concentration likely gives higher concentrations of **1**. Fibers may form with a combination of **1** and **1P**. Hence higher relative concentrations of **1** would likely give fibers with a higher composition of **1** relative to **1P**, leading to more stable structures.

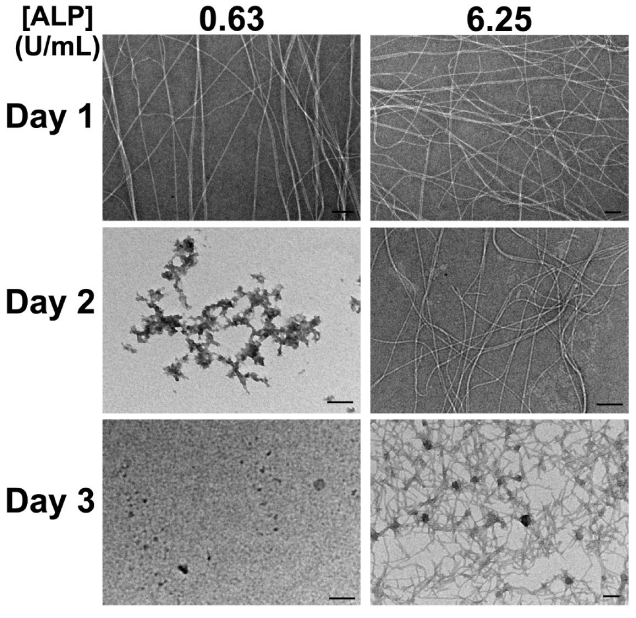

Figure 6. TEM micrographs taken on three consecutive days of suspensions of **1P**, **2**, and ALP with varying concentrations of ALP. $[\mathbf{1P}]_0$ = [**2**] = 500 μM, pH = 7.6, each scale bar is 100 nm.

In addition, dynamic oscillatory rheology confirms the disintegration of the gels formed by dephosphorylation of **1P** in the presence of **2** and ALP. While both the storage and loss moduli are frequency independent, the storage and loss moduli of the gels formed by EISA of a solution of 500 μM **1P** with 1.25 U/mL ALP in the presence of 1 equiv of **2** decrease about an order of magnitude from 24 to 48 h (Figures S3 and S4), indicating that **2** promotes the dissociation of the gel matrix. Hence both rheology and TEM confirm that the self-assembled fibers are a transient structure, indicative of a local energy minimum, with binding and subsequent precipitation of **1** and **2** being the global energy minimum.

Modulation of the Free Energy Landscape. The transient formation of the nanofibers during EISA and the relative stability of assemblies of **1** against further precipitation after the addition of **2** indicate the presence of multiple structurally diverse intermediates along the fibril formation pathway. These intermediates likely interact with **2** to divert self-assembly away from fibril formation. Specifically, transient formation of nanofibers upon EISA of **1P** and further deterioration of assembled **1** into a precipitate of **1** and **2**, together with the observation that the addition of Tw-80 disrupts assemblies of **1** and restores binding between **1** and **2**, indicate that either (i) common di-, tri-, or oligomeric intermediates of **1** exist for both nanofiber assembly and precipitation or (ii) these pathways share only monomeric **1**. Figure 7 illustrates the plausible energy landscape for EISA of **1P** both in the presence and absence of **2**. Containing an enzyme-catalyzed step, EISA is inherently under kinetic control, and hence observations at thermodynamic equilibrium offer little information on perturbation of EISA by **2**. However, analysis of time-dependent TEM, ITC, and the responses of the system to different concentrations of ligand provide insights

DOI: 10.1021/jacs.6b07677
J. Am. Chem. Soc. 2016, 138, 15397−15404

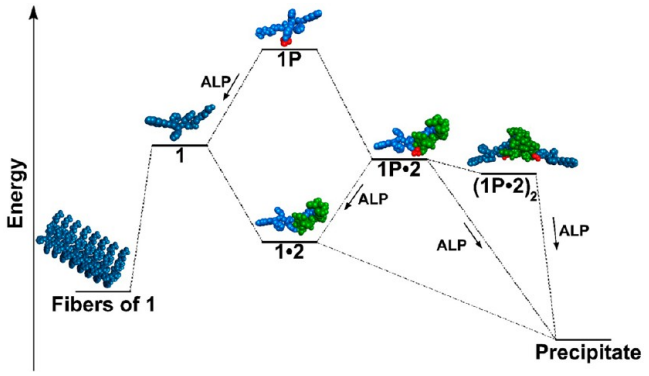

Figure 7. Qualitative energy landscape for the multiple paths of the assembly or precipitation of **1** and **2** based on thermodynamic data from ITC and relative stabilities of assemblies from TEM studies showing the role of **2** in stabilizing precipitation pathways. Oligomers of **1P** and **1** which likely exist are left out for clarity.

into these kinetic pathways. Without **2**, EISA of **1P** follows a simple pathway illustrated on the left of Figure 7, whereby **1P** (or oligomeric **1P**) first undergoes dephosphorylation to provide **1**, which further assembles to form nanofibrils. Although it is possible that **1P** may form micelles before dephosphorylation,[54] such a scenario is less likely in the presence of **2** because **2** binds to **1P** and disfavors the formation of micelle (as shown in Figure 1A). However, in the presence of **2**, the entire energy landscape appears to be available, yielding a complex mixture of species. **1P** may bind with **2** in solution creating a lower energy species (**1P·2**) than simply "monomeric" **1P**, which can be further dephosphorylated to form **1·2**, and may further assemble to yield precipitates. Additionally, as dimerization of **2** is well-known,[35] a dimeric complex $(\mathbf{1P{\cdot}2})_2$ of **2** and **1P** and/or **1** is likely to form instead of the complex (**1P·2**), which further aggregates following dephosphorylation to form a precipitate. Aggregation is likely driven by the high local concentration of **2** caused by dimerization and perhaps also by the ability for **2** to promote dimerization of a peptide hydrogelator, as we have previously shown.[44] The results in Figure 5 indicate that more than 1 equiv of **2** is needed for the formation of the precipitate and **2** is part of the precipitate, thus **2** unlikely catalyzes the fiber to precipitate conversion. Importantly, when vancomycin aglycon[55,56] replaces **2**, no aggregates were observed (Figure S20); however, short fibers similar to those in Figure 5 were observed, indicating that vancomycin aglycon destabilizes assemblies of **1** in a similar fashion to **2**. Because the glycogen of **2** is essential for dimerization in water, this result indicates that dimerization of **2** allows the formation of large structures, thereby promoting further aggregation. In addition, this observation supports formation of the dimeric complex $(\mathbf{1P{\cdot}2})_2$ as a key intermediate in the precipitation pathway. Therefore, during EISA of **1P**, the presence of **2** allows for formation of lower energy complexes with **1P** or **1**, diverting the supramolecular aggregation by creating a lower energy pathway, similar to molecular catalysts or molecular chaperones.[57]

In addition to **2** diverting assembly of **1** during EISA, TEM reveals that **2** destabilizes the assemblies of **1**. The addition of 1 equiv of **2** to the nanofibers of **1** is unable to lead to precipitation (Figure 1D), while the addition of 5 equiv of **2** to nanosheets of **1** gives an opaque colloidal suspension paired with disruption of the nanosheets of **1** (Figure S4). Additionally, binding between **1** and **2** is restored upon the addition of Tw-80 that breaks up assemblies of **1**, as evidenced by ITC (Figure 2d) and TEM (Figure 4), indicating that **1** and **2** can interact. Hence although assemblies of **1** barely revert to oligomers or monomers that can bind with **2**, sufficiently high concentrations of **2** can perturb the energy landscape and pull the equilibrium toward binding of **1** and **2**. Based on this, there are two plausible "mechanisms" for **2** breaking the assemblies of **1**: (i) Free **2** in solution can bind with monomeric or oligomeric **1** and initiate precipitation, thereby lowering the concentration of **1** in solution, leading to deterioration of large assemblies of **1**; and (ii) **2** may bind directly to assemblies of **1** leading to destruction of the assemblies and formation of an intermediate species of **1** and **2**, followed by precipitate formation. Direct binding of **2** to the assemblies of **1**, however, is unlikely as ITC showed little release of heat upon titration of **2** to assembled **1** (Figure 2b). Hence precipitation caused by **2** relies either on reversible supramolecular polymerization of **1** or on the presence of intermediate species of **1** in solution. Therefore, transient formation of fibers of **1** is indicative of the dynamic nature of EISA, a process that dynamically evolves based on atomistic interactions between precursors (**1P**) of the self-assembling molecules (**1**) as well as ligands (**2**), eventually bringing the system to kinetic or thermal equilibrium dependence on both the initial and boundary conditions of the system.

CONCLUSION

The assembly or aggregation of proteins or peptides remains one of the most significant problems in biology and medicine, especially associated with diseases like Alzheimer's disease.[58−63] The path taken, however, depends strongly on the initial conditions of the system as well as intrinsic kinetic factors such as enzyme activation or critical nucleus formation. Recently, ionic strength was found to modulate the energy landscape of $A\beta_{40}$.[51] However, control over peptide concentration and initial state remains difficult.[51] While it remains to prove that ligand−receptor interactions may modulate the aggregation of $A\beta$,[50] this study on how interaction with a ligand significantly alters supramolecular assembly of small molecules should provide useful insights. Because the formation of $A\beta$ results from enzymatic reactions,[64,65] the study of ligand−receptor interactions to modulate EISA of small molecules is more relevant to the disease condition than using hexafluoroisopropanol (HFIP) or dimethyl sulfoxide to generate $A\beta$ amyloids.[66] In fact, we used HFIP to form the nanofibers of **1** and found that using HFIP leads to various different morphologies (Figure S21).

Moreover, it is well-known that in drug screening, small molecules hit with high aggregation potentials are poor candidates due to unpredictable efficacy of ligand−receptor interactions.[45,46] This fact not only implies that self-assembly of small molecules should modulate specific ligand−receptor interactions but also suggests a limited knowledge about the molecular interactions between aggregates and their target molecules. EISA creates multiple processes which run in parallel, while also providing control over aggregating peptide concentration. Additionally, this experimental system should be useful for the study of the kinetics of the interconversion of the molecular species, though one has to obtain accurate rate information on the reactions.

Although being extensively used by nature for controlling important cellular functions such as apoptosis[67] and immune

DOI: 10.1021/jacs.6b07677
J. Am. Chem. Soc. 2016, 138, 15397−15404

responses,[68] exploration of EISA in the context of small molecules is at its infancy.[26,69−77] Recently, EISA has found applications in selective inhibition of cancer cells[22,78−82] or targeting tumors in an animal model,[83] but enzymatic control over ligand−receptor interactions of small molecules has yet to be investigated. This work, thus, provides necessary understanding to develop EISA in sophisticated environments with prevailing ligand−receptor interactions. Hence, this study demonstrates that perturbation of assembly can be accomplished through modulation of the relative energies of intermediate species. In a more general sense, the insights obtained in this work would contribute to the exploration of supramolecular chemistry in cellular milieu.

■ ASSOCIATED CONTENT

Supporting Information

The Supporting Information is available free of charge on the ACS Publications website at DOI: 10.1021/jacs.6b07677.

Details of the synthesis, TEM images, and ITC (PDF)

■ AUTHOR INFORMATION

Corresponding Author

*bxu@brandeis.edu

Author Contributions

†These authors contributed equally.

Notes

The authors declare no competing financial interest.

■ ACKNOWLEDGMENTS

This work was partially supported by NIH (R01CA142746), NSF (MRSEC-1420382), and the W. M. Keck Foundation.

■ REFERENCES

(1) *Comprehensive Supramolecular Chemistry: Templating, self-assembly, and self-organization*; Atwood, J. L., Davies, J. E. D., MacNicol, D. D., Vögtle, F., Eds.; Pergamon: Oxford, 1996; Vol. 9.
(2) Fréchet, J. M. J. *Proc. Natl. Acad. Sci. U. S. A.* **2002**, *99*, 4782.
(3) Kato, T. *Science* **2002**, *295*, 2414.
(4) Whitesides, G. M.; Grzybowski, B. *Science* **2002**, *295*, 2418.
(5) Aida, T.; Meijer, E. W.; Stupp, S. I. *Science* **2012**, *335*, 813.
(6) Liu, J.; Morikawa, M.-a.; Kimizuka, N. *J. Am. Chem. Soc.* **2011**, *133*, 17370.
(7) Wong, K. M.-C.; Yam, V. W.-W. *Acc. Chem. Res.* **2011**, *44*, 424.
(8) Po, C.; Tam, A. Y.-Y.; Wong, K. M.-C.; Yam, V. W.-W. *J. Am. Chem. Soc.* **2011**, *133*, 12136.
(9) Kato, T.; Kihara, H.; Kumar, U.; Uryu, T.; Fréchet, J. M. J. *Angew. Chem., Int. Ed. Engl.* **1994**, *33*, 1644.
(10) Boekhoven, J.; Hendriksen, W. E.; Koper, G. J. M.; Eelkema, R.; van Esch, J. H. *Science* **2015**, *349*, 1075.
(11) Pezzato, C.; Prins, L. J. *Nat. Commun.* **2015**, *6*, 7790.
(12) Graves, J. D.; Krebs, E. G. *Pharmacol. Ther.* **1999**, *82*, 111.
(13) Turner, M.; Billadeau, D. D. *Nat. Rev. Immunol.* **2002**, *2*, 476.
(14) Craig, E. A.; Weissman, J. S.; Horwich, A. L. *Cell* **1994**, *78*, 365.
(15) Horst, R.; Horwich, A. L.; Wüthrich, K. *J. Am. Chem. Soc.* **2011**, *133*, 16354.
(16) Sun, L.; Wang, H.; Wang, Z.; He, S.; Chen, S.; Liao, D.; Wang, L.; Yan, J.; Liu, W.; Lei, X.; Wang, X. *Cell* **2012**, *148*, 213.
(17) Shi, J.; Du, X.; Yuan, D.; Haburcak, R.; Wu, D.; Zhou, N.; Xu, B. *Chem. Commun.* **2015**, *51*, 4899.
(18) Williams, R. J.; Smith, A. M.; Collins, R.; Hodson, N.; Das, A. K.; Ulijn, R. V. *Nat. Nanotechnol.* **2009**, *4*, 19.
(19) Komatsu, H.; Matsumoto, S.; Tamaru, S.-i.; Kaneko, K.; Ikeda, M.; Hamachi, I. *J. Am. Chem. Soc.* **2009**, *131*, 5580.
(20) Gao, J.; Wang, H.; Wang, L.; Wang, J.; Kong, D.; Yang, Z. *J. Am. Chem. Soc.* **2009**, *131*, 11286.
(21) Zhang, Y.; Gu, H.; Yang, Z.; Xu, B. *J. Am. Chem. Soc.* **2003**, *125*, 13680.
(22) Tanaka, A.; Fukuoka, Y.; Morimoto, Y.; Honjo, T.; Koda, D.; Goto, M.; Maruyama, T. *J. Am. Chem. Soc.* **2015**, *137*, 770.
(23) Zhou, J.; Du, X.; Berciu, C.; He, H.; Shi, J.; Nicastro, D.; Xu, B. *Chem.* **2016**, *1*, 246.
(24) Kuang, Y.; Gao, Y.; Xu, B. *Chem. Commun.* **2011**, *47*, 12625.
(25) Ye, D.; Shuhendler, A. J.; Cui, L.; Tong, L.; Tee, S. S.; Tikhomirov, G.; Felsher, D. W.; Rao, J. *Nat. Chem.* **2014**, *6*, 519.
(26) Li, J.; Gao, Y.; Kuang, Y.; Shi, J.; Du, X.; Zhou, J.; Wang, H.; Yang, Z.; Xu, B. *J. Am. Chem. Soc.* **2013**, *135*, 9907.
(27) Gao, Y.; Berciu, C.; Kuang, Y.; Shi, J.; Nicastro, D.; Xu, B. *ACS Nano* **2013**, *7*, 9055.
(28) Hughes, M.; Frederix, P. W. J. M.; Raeburn, J.; Birchall, L. S.; Sadownik, J.; Coomer, F. C.; Lin, I. H.; Cussen, E. J.; Hunt, N. T.; Tuttle, T.; Webb, S. J.; Adams, D. J.; Ulijn, R. V. *Soft Matter* **2012**, *8*, 5595.
(29) Zhou, J.; Xu, B. *Bioconjugate Chem.* **2015**, *26*, 987.
(30) Shi, J.; Xu, B. *Nano Today* **2015**, *10*, 615.
(31) Bah, A.; Vernon, R. M.; Siddiqui, Z.; Krzeminski, M.; Muhandiram, R.; Zhao, C.; Sonenberg, N.; Kay, L. E.; Forman-Kay, J. D. *Nature* **2015**, *519*, 106.
(32) Fisher, C. K.; Huang, A.; Stultz, C. M. *J. Am. Chem. Soc.* **2010**, *132*, 14919.
(33) Walsh, C. T.; Fisher, S. L.; Park, I. S.; Prahalad, M.; Wu, Z. *Chem. Biol.* **1996**, *3*, 21.
(34) Walsh, C. T. *Antibiotics: Actions, origins, resistance*; ASM Press: Washington, DC, 2003.
(35) Williams, D. H.; Maguire, A. J.; Tsuzuki, W.; Westwell, M. S. *Science* **1998**, *280*, 711.
(36) Rao, J. H.; Lahiri, J.; Isaacs, L.; Weis, R. M.; Whitesides, G. M. *Science* **1998**, *280*, 708.
(37) Rao, J. H.; Yan, L.; Xu, B.; Whitesides, G. M. *J. Am. Chem. Soc.* **1999**, *121*, 2629.
(38) Sundram, U. N.; Griffin, J. H.; Nicas, T. I. *J. Am. Chem. Soc.* **1996**, *118*, 13107.
(39) Leimkuhler, C.; Chen, L.; Barrett, D.; Panzone, G.; Sun, B. Y.; Falcone, B.; Oberthur, M.; Donadio, S.; Walker, S.; Kahne, D. *J. Am. Chem. Soc.* **2005**, *127*, 3250.
(40) Shi, J.; Du, X.; Huang, Y.; Zhou, J.; Yuan, D.; Wu, D.; Zhang, Y.; Haburcak, R.; Epstein, I. R.; Xu, B. *J. Am. Chem. Soc.* **2015**, *137*, 26.
(41) Shi, J.; Du, X.; Yuan, D.; Haburcak, R.; Zhou, N.; Xu, B. *Bioconjugate Chem.* **2015**, *26*, 1879.
(42) *Fmoc Solid Phase Peptide Synthesis: A Practical Approach*; Chan, W. C., White, P. D., Eds.; Oxford University Press Inc.: Oxford, 2000.
(43) Alewood, P. F.; Johns, R. B.; Valerio, R. M.; Kemp, B. E. *Synthesis* **1983**, *1983*, 30.
(44) Zhang, Y.; Yang, Z. M.; Yuan, F.; Gu, H. W.; Gao, P.; Xu, B. *J. Am. Chem. Soc.* **2004**, *126*, 15028.
(45) Irwin, J. J.; Duan, D.; Torosyan, H.; Doak, A. K.; Ziebart, K. T.; Sterling, T.; Tumanian, G.; Shoichet, B. K. *J. Med. Chem.* **2015**, *58*, 7076.
(46) McGovern, S. L.; Helfand, B. T.; Feng, B.; Shoichet, B. K. *J. Med. Chem.* **2003**, *46*, 4265.
(47) Teunissen, A. J. P.; Paffen, T. F. E.; Ercolani, G.; de Greef, T. F. A.; Meijer, E. W. *J. Am. Chem. Soc.* **2016**, *138*, 6852.
(48) van der Zwaag, D.; Pieters, P. A.; Korevaar, P. A.; Markvoort, A. J.; Spiering, A. J. H.; de Greef, T. F. A.; Meijer, E. W. *J. Am. Chem. Soc.* **2015**, *137*, 12677.
(49) Teunissen, A. J. P.; Nieuwenhuizen, M. M. L.; Rodríguez-Llansola, F.; Palmans, A. R. A.; Meijer, E. W. *Macromolecules* **2014**, *47*, 8429.
(50) Garai, K.; Verghese, P. B.; Baban, B.; Holtzman, D. M.; Frieden, C. *Biochemistry* **2014**, *53*, 6323.
(51) Abelein, A.; Jarvet, J.; Barth, A.; Gräslund, A.; Danielsson, J. *J. Am. Chem. Soc.* **2016**, *138*, 6893.

DOI: 10.1021/jacs.6b07677
J. Am. Chem. Soc. 2016, 138, 15397−15404

(52) Kurouski, D.; Lu, X.; Popova, L.; Wan, W.; Shanmugasundaram, M.; Stubbs, G.; Dukor, R. K.; Lednev, I. K.; Nafie, L. A. *J. Am. Chem. Soc.* **2014**, *136*, 2302.
(53) Hirst, A. R.; Roy, S.; Arora, M.; Das, A. K.; Hodson, N.; Murray, P.; Marshall, S.; Javid, N.; Sefcik, J.; Boekhoven, J.; van Esch, J. H.; Santabarbara, S.; Hunt, N. T.; Ulijn, R. V. *Nat. Chem.* **2010**, *2*, 1089.
(54) Thornton, K.; Abul-Haija, Y. M.; Hodson, N.; Ulijn, R. V. *Soft Matter* **2013**, *9*, 9430.
(55) Xie, J.; Okano, A.; Pierce, J. G.; James, R. C.; Stamm, S.; Crane, C. M.; Boger, D. L. *J. Am. Chem. Soc.* **2012**, *134*, 1284.
(56) Xie, J.; Pierce, J. G.; James, R. C.; Okano, A.; Boger, D. L. *J. Am. Chem. Soc.* **2011**, *133*, 13946.
(57) Hartl, F. U. *Nature* **1996**, *381*, 571.
(58) Wang, J.; Zhao, C.; Zhao, A.; Li, M.; Ren, J.; Qu, X. *J. Am. Chem. Soc.* **2015**, *137*, 1213.
(59) Hamley, I. W. *Chem. Rev.* **2012**, *112*, 5147.
(60) Economou, N. J.; Giammona, M. J.; Do, T. D.; Zheng, X.; Teplow, D. B.; Buratto, S. K.; Bowers, M. T. *J. Am. Chem. Soc.* **2016**, *138*, 1772.
(61) Zhu, L.; Song, Y.; Cheng, P.-N.; Moore, J. S. *J. Am. Chem. Soc.* **2015**, *137*, 8062.
(62) Colvin, M. T.; Silvers, R.; Frohm, B.; Su, Y.; Linse, S.; Griffin, R. G. *J. Am. Chem. Soc.* **2015**, *137*, 7509.
(63) Murphy, M. P.; LeVine, H. *J. Alzheimer's Dis.* **2010**, *19*, 311.
(64) Sisodia, S. S., St; George-Hyslop, P. H. *Nat. Rev. Neurosci* **2002**, *3*, 281.
(65) Chow, V. W.; Mattson, M. P.; Wong, P. C.; Gleichmann, M. *NeuroMol. Med.* **2010**, *12*, 1.
(66) Stine, W. B.; Jungbauer, L.; Yu, C.; LaDu, M. J. In *Alzheimer's Disease and Frontotemporal Dementia: Methods and Protocols*; Roberson, D. E., Ed.; Humana Press: Totowa, NJ, 2011; p 13.
(67) Ashkenazi, A.; Dixit, V. M. *Science* **1998**, *281*, 1305.
(68) Lu, A.; Magupalli, V. G.; Venkat, G.; Ruan, J.; Yin, Q.; Atianand, M. K.; Vos, M. R.; Schröder, G. F.; Fitzgerald, K. A.; Wu, H.; Egelman, E. H. *Cell* **2014**, *156*, 1193.
(69) Toledano, S.; Williams, R. J.; Jayawarna, V.; Ulijn, R. V. *J. Am. Chem. Soc.* **2006**, *128*, 1070.
(70) Yang, Z.; Liang, G.; Xu, B. *Acc. Chem. Res.* **2008**, *41*, 315.
(71) Yang, Z. M.; Ho, P. L.; Liang, G. L.; Chow, K. H.; Wang, Q. G.; Cao, Y.; Guo, Z. H.; Xu, B. *J. Am. Chem. Soc.* **2007**, *129*, 266.
(72) Zhou, J.; Du, X.; Gao, Y.; Shi, J.; Xu, B. *J. Am. Chem. Soc.* **2014**, *136*, 2970.
(73) Zhou, J.; Du, X.; Li, J.; Yamagata, N.; Xu, B. *J. Am. Chem. Soc.* **2015**, *137*, 10040.
(74) Li, J.; Kuang, Y.; Gao, Y.; Du, X.; Shi, J.; Xu, B. *J. Am. Chem. Soc.* **2013**, *135*, 542.
(75) Gao, Y.; Kuang, Y.; Guo, Z.-F.; Guo, Z.; Krauss, I. J.; Xu, B. *J. Am. Chem. Soc.* **2009**, *131*, 13576.
(76) Yang, Z. M.; Liang, G. L.; Wang, L.; Xu, B. *J. Am. Chem. Soc.* **2006**, *128*, 3038.
(77) Yang, Z.; Gu, H.; Fu, D.; Gao, P.; Lam, J. K.; Xu, B. *Adv. Mater.* **2006**, *18*, 545.
(78) Kuang, Y.; Shi, J.; Li, J.; Yuan, D.; Alberti, K. A.; Xu, Q.; Xu, B. *Angew. Chem., Int. Ed.* **2014**, *53*, 8104.
(79) Yang, Z.; Liang, G.; Guo, Z.; Guo, Z.; Xu, B. *Angew. Chem., Int. Ed.* **2007**, *46*, 8216.
(80) Shi, J.; Du, X.; Yuan, D.; Zhou, J.; Zhou, N.; Huang, Y.; Xu, B. *Biomacromolecules* **2014**, *15*, 3559.
(81) Pires, R. A.; Abul-Haija, Y. M.; Costa, D. S.; Novoa-Carballal, R.; Reis, R. L.; Ulijn, R. V.; Pashkuleva, I. *J. Am. Chem. Soc.* **2015**, *137*, 576.
(82) Li, J.; Kuang, Y.; Shi, J.; Zhou, J.; Medina, J. E.; Zhou, R.; Yuan, D.; Yang, C.; Wang, H.; Yang, Z.; Liu, J.; Dinulescu, D. M.; Xu, B. *Angew. Chem., Int. Ed.* **2015**, *54*, 13307.
(83) Huang, P.; Gao, Y.; Lin, J.; Hu, H.; Liao, H.-S.; Yan, X.; Jin, A.; Tang, Y.; Song, J.; Niu, G.; Zhang, G.; Horkay, F.; Chen, X. *ACS Nano* **2015**, *9*, 9517.

DOI: 10.1021/jacs.6b07677
J. Am. Chem. Soc. 2016, 138, 15397−15404